AGU PUBLICATIONS

Geophysical Research Letters

RESEARCH LETTER
10.1002/2017GL072711

Key Points:
- We statistically investigate stratigraphic relationships of impact craters and thrust faults on Mercury
- Stratigraphic relationships contain information on timing and rate of Mercury's radius decrease
- Results permit calculation of strain and strain rate of global contraction during each of Mercury's time-stratigraphic systems

Supporting Information:
- Supporting Information S1
- Data S1
- Data S2
- Data S3
- Movie S1

Correspondence to:
K. T. Crane,
kelsey.crane@uga.edu

Citation:
Crane, K. T., and C. Klimczak (2017), Timing and rate of global contraction on Mercury, *Geophys. Res. Lett.*, *44*, 3082–3089, doi:10.1002/2017GL072711.

Received 18 AUG 2016
Accepted 21 MAR 2017
Accepted article online 27 MAR 2017
Published online 15 APR 2017

Timing and rate of global contraction on Mercury

Kelsey T. Crane[1] and **Christian Klimczak**[1]

[1]Structural Geology and Geomechanics Group, Department of Geology, University of Georgia, Athens, Georgia, USA

Abstract Impact bombardment and global contraction due to planetary cooling have both shaped the surface of Mercury over very long time scales. Landforms associated with these processes, i.e., impact craters and thrust fault-related escarpments, and their mutual geologic relationships were analyzed to gain insight into the temporal relationships between the two. We assess stratigraphic relationships of ~6000 thrust fault-related landforms with all 20 km diameter and larger craters to statistically evaluate the timing and rate of contraction on Mercury. Geometric probabilities were computed for thrust faults crosscutting craters of different degradation stages that correspond to different time-stratigraphic systems, which allow determination of the onset and time derivative of global contraction. Results show that this process had begun after the late heavy bombardment of the inner solar system and likely gradually slowed toward the present. Implications arise for thermal history models as well as slip rates and quake recurrence intervals along thrust faults on Mercury.

1. Mercury's Record of Craters and Thrust Faults

Thrust faulting caused by planetary cooling and associated global contraction [*Solomon*, 1977] and impact cratering [*Morbidelli et al.*, 2012; *Marchi et al.*, 2013] are two processes that have modified Mercury's surface throughout much of its geologic past. Thrust faulting is known to produce positive-relief linear to arcuate ridges. More than 6000 such landforms have previously been mapped and, when related to a given set of subsurface fault geometries, are estimated to accommodate a 3.1 to 7.1 km planetary radius decrease [*Byrne et al.*, 2014]. Thrust fault activity caused by global contraction on Mercury was found by both thermal modeling and geologic studies to have begun by or near the end of the late heavy bombardment (LHB) of the inner solar system [*Hauck et al.*, 2004; *Tosi et al.*, 2013; *Banks et al.*, 2015a].

The slow and incremental development of relief associated with thrust faults stands in stark contrast to the nearly instantaneous formation of impact craters. During and before the LHB, the vast majority of Mercury's craters and basins formed, with fewer large craters emplaced in recent times [*Morbidelli et al.*, 2012]. While the well-studied cratering record and rate on the Moon [e.g., *Trask*, 1967] have motivated investigations into cratering fluxes [*Strom and Neukum*, 1988; *Marchi et al.*, 2013] and crater morphology [e.g., *Trask*, 1971; *Trask and Guest*, 1975; *Spudis and Guest*, 1988] the onset and especially the rate of global contraction have not been approached with such rigor. However, results of thermal evolution models produce a wide range of solutions for contraction amount, onset, and rates [e.g., *Hauck et al.*, 2004; *Grott et al.*, 2011; *Tosi et al.*, 2013] that can be compared to geologic observations. Using MErcury Surface, Space, ENvironment, GEochemistry, and Ranging (MESSENGER) data, we establish and statistically investigate stratigraphic relationships of impact craters and basins with all detected thrust faults to deduce the timing and rate at which global contraction operated throughout Mercury's geologic history. These results are then used to calculate variations in contraction rate over time that have acute implications for thermal models.

1.1. Craters and Mercury's Stratigraphy

Mercury's craters vary in size and morphology, ranging from large, heavily degraded basins to small, morphologically crisp craters. This observation has led to categorization of impact structures into five morphologic classes since the return of Mariner 10 images [*Wood et al.*, 1977; *McCauley et al.*, 1981; *Barnouin et al.*, 2012]. Recently, *Kinczyk et al.* [2016] categorized all craters greater than 40 km in diameter by using MESSENGER data. Their classification scheme closely followed that described by *Spudis and Guest* [1988] in which craters belonging to classes 1 and 2 are the most degraded, with discontinuous rims and many superposing craters (Figures 1a and 1b). Class 3 craters show slumped wall terraces, central peaks, and fewer superposing craters (Figures 1c and 1d), class 4 craters have well defined peaks and slightly degraded rim crests and terraces (Figures 1e and 1f), and class 5 craters, the least degraded of all craters on Mercury, have the

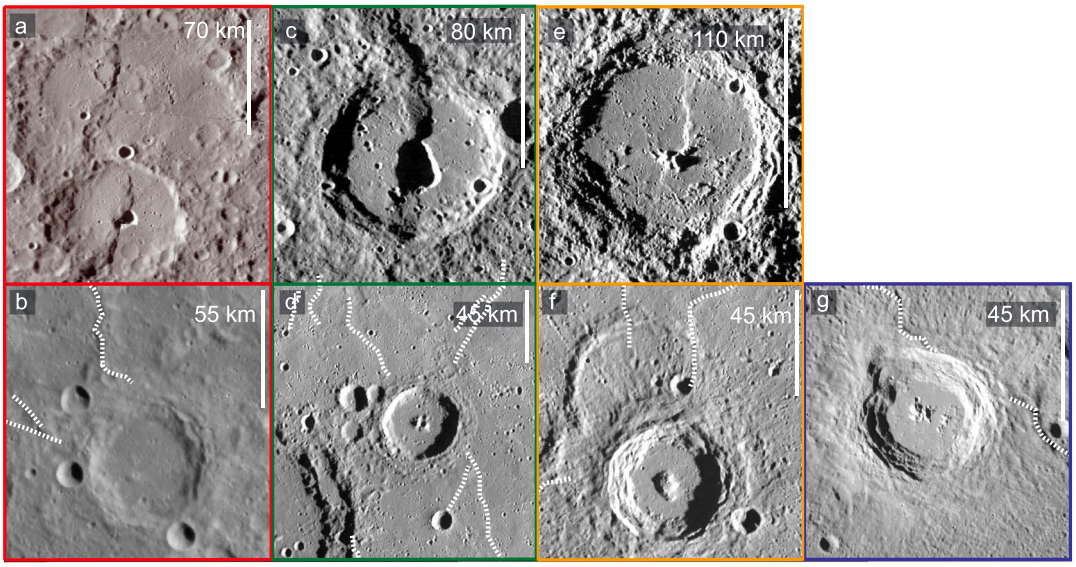

Figure 1. Stratigraphic relationships between faults and craters include craters cut by faults and craters superposing faults. (a) Tolstojan crater "Rumi" centered at 105°W, 24°S superposing an unnamed Pre-Tolstojan crater. Sometime after emplacement, both craters were cut by Palmer Rupes. (b) An unnamed Tolstojan crater centered at 53°E, 40°S potentially superposing three degraded thrust fault-related landforms. (c) The Calorian crater "Geddes" located at 30°W, 27°N cut by Antoniadi Dorsum. (d) An unnamed Calorian crater superposing a thrust fault-related landform located at 17°E, 45.5°N. (e) Mansurian crater "Ts'ai Wen-Chi" located at 23°W, 23°N cut by an unnamed thrust fault-related landform. (f and g) Unnamed Mansurian and Kuiperian craters centered at 13°E, 49°N and 65°E, 48°N, respectively, superposing unnamed thrust fault-related landforms. Degradation stages of all craters shown here were classified originally by *Spudis and Guest* [1988] and most recently by *Kinczyk et al.* [2016].

same characteristics as class 4 craters but also display rays and lighter colored ejecta (Figure 1g). These five classes are generally interpreted to coincide with Mercury's five time-stratigraphic systems: (1) the Pre-Tolstojan (>~4 Ga), (2) Tolstojan (~4–3.9 Ga), (3) Calorian (3.9 – ~3.5 to 3 Ga), (4) Mansurian (~3.5 to 3 Ga–1 Ga), and (5) Kuiperian (<1 Ga) [*Spudis and Guest*, 1988], but recent investigations found that there may be greater variability in the absolute ages of these systems than previously established [*Braden and Robinson*, 2013; *Banks et al.*, 2016].

1.2. Stratigraphic Relationships of Craters With Thrust Faults

We conducted a geospatial analysis to locate where thrust faults and craters showed stratigraphic relationships and distinguished between craters that are cut by faults and those that superpose faults (see supporting information for details). Craters cut by faults (Figures 1a, 1c, and 1e) must have been emplaced before or at a time of active thrust faulting, whereas craters superposing faults (Figures 1b, 1d, and 1g) supersede thrust fault activity at that location. The oldest superposing craters mark the earliest evidence for thrust fault activity and thus provide a lower bound for the onset of global contraction. Importantly, faulting is a long-lived, periodic process [*Cowie and Scholz*, 1992], and so a fault deforming a Tolstojan crater, for example, may have developed as early as the Tolstojan but could have formed or accommodated strain during any subsequent period as well. Thrust fault-related landforms could have also existed prior to the impact event and may have partly or entirely been erased by the cratering process. But the age of a crater deformed by a fault nevertheless provides information on the time during or after which the fault was active, irrespective of whether some portion of that fault could have existed prior to the impact event.

Kinczyk et al. [2016] mapped craters as small as 20 km and classified craters with diameters greater than 40 km. We classified the 20 to 40 km diameter craters that displayed stratigraphic relationships with faults by using global MESSENGER image mosaics. From a total of 3112 craters and basins ranging from 20 to 2000 km in diameter, 2310 structures were categorized into classes 1 and 2 [*Kinczyk et al.*, 2016], placing their formation likely during or before the Tolstojan [*Spudis and Guest*, 1988]. Of this combined subset of craters, 1196 were spatially correlated with faults, with 1192 cut (Figure 1a), and four interpreted to be superposing faults (Figure 1b). The combination of a rapid early cratering rate with so few

fault-superposing craters indicates that most faults formed after these craters were emplaced and thus that thrust faulting may have been active but was likely not a planet-wide process before and during this time-stratigraphic system. Among 536 identified class 3 craters, 370 craters were spatially associated with faults, where 266 were cut (Figure 1c) and 104 superposed faults (Figure 1d). Class 3 craters are widely thought to have been emplaced during the Calorian, and the number of fault-superposing class 3 craters shows that a substantial amount of faulting must have occurred prior to the emplacement of craters of this class. This relationship indicates that thrust faulting was well underway during this time-stratigraphic system and so marks an increase in contractional tectonic activity following the Tolstojan. Of 244 identified class 4 craters, 104 were associated spatially with faults, where 49 were cut (Figure 1e) and 55 superposed faults (Figure 1f). Craters with such morphological characteristics are thought to have been emplaced during the Mansurian. Because over half of these craters superpose faults, substantial faulting must have occurred before the end of the Mansurian, with some faulting potentially occurring after. The increasing proportions of craters superposing faults indicate that global contraction, although active during the Mansurian, had likely slowed. The influx of large impactors had also decreased by this time, so relative percentages of stratigraphic relationships are used in our analysis instead of absolute counts (further discussed in section 2). Of 22 identified class 5 craters only three were associated spatially with thrust faults; all of them superposed a fault (Figure 1g). With a low impact flux during the Kuiperian, the time-stratigraphic system during which class 5 craters are thought to have been emplaced, it is statistically unlikely that craters of this category would be associated spatially with a fault. Given the numerical relationship of these craters to faults, however, thrust fault activity induced by global contraction was low across Mercury's surface during this system. These relationships agree with a previous, qualitative assessment of stratigraphic relationships of craters and thrust faults [*Banks et al.*, 2015a].

2. Timing of Thrust Faulting

The thrust fault-related landforms superposed by craters cannot be younger than the craters themselves, providing evidence that global contraction was underway at the time such craters formed. Out of a total population of 2310 preserved craters likely emplaced during and before the Tolstojan, we located only four craters that we interpret to superpose faults. Such a small number of craters indicates that although fault activity potentially predated the crater formation and thus occurred within this time system, the activity only occurred in isolated localities. Arguably, evidence for Pre-Tolstojan and Tolstojan thrust fault-related landforms and their stratigraphic relationships with craters—if present—may have been erased from the geologic record. But given that large fault-related landforms likely degrade at rates comparable to crater rims and the large number of preserved crater rims from that time, it is unlikely that only four such relationships were preserved if faulting had been a widespread and active process during and before the Tolstojan. The much higher number of fault-superposing craters in the Calorian instead indicates that thrust faulting and thus global contraction were well underway during this time-stratigraphic system. Prior to the onset of thrust faulting, however, the lithosphere likely elastically supported an initial radius decrease from cooling of up to 2.1 km [*Klimczak*, 2015], showing that global contraction was likely initiated prior to the Calorian already.

We statistically verified that the geographic distribution of craters across Mercury is similar throughout each time system and evaluated the geographic distribution of thrust fault-related landforms with a Bootstrap (repeated cluster) analysis (see supporting information). Tidal despinning and variations in crustal thickness may produce a nonrandom (clustered) fault distribution [*Watters et al.*, 2015]. Our analysis identifies a uniform distribution of thrust fault-related landforms with clusters only present in Mercury's smooth plains units. Faults within these clusters do not form enough stratigraphic relationships with craters to significantly impact our results (see supporting information). For a uniformly distributed population of thrust faults, one would expect that the population of craters present at the onset of global thrust fault activity would be more or less equally affected by the faults and that different subpopulations of craters would display that same relationship. The ratios of cut craters to total craters emplaced during the Pre-Tolstojan, Tolstojan, and Calorian systems are 0.53, 0.50, and 0.49, respectively. The ratios drop noticeably for the Mansurian (0.2) and Kuiperian (0). These numbers reflect that the first three populations of craters were likely exposed to the same degree of faulting, showing once more that thrust faulting likely began during the Calorian. The decrease in these ratios for the Mansurian and Kuiperian systems indicates that a substantial amount of the fault activity had already occurred before these time-stratigraphic systems, with the Kuiperian being tectonically quiet

(supported in more detail in section 3). Evidence for local, small-scale thrust fault activity, however, was interpreted to have occurred during the Kuiperian to as recent as 50 Ma ago [*Banks et al.*, 2015a; *Watters et al.*, 2016], but as our statistical analysis focuses on craters with diameters of 20 km and larger, any small-scale fault activity is not captured with our approach.

3. Strain and Strain Rate

Strain is a measure of deformation of an object relative to its original size. For a contracting planet, the term refers to its radius change compared to the radius of the planet prior to contraction. The permanent, brittle strain Mercury's lithosphere experienced from global contraction was accommodated by many thrust faults. For a geographically uniformly distributed population of faults (see supporting information), larger and older craters have greater probabilities of being spatially associated with thrust faults. For example, Pre-Tolstojan and Tolstojan craters, which have been exposed on Mercury's surface for billions of years, have a much greater probability of being spatially associated with thrust faults than younger, generally smaller Mansurian or Kuiperian craters.

Stratigraphic relationships between craters and faults are determined by geometric probabilities and are a function of the cratering rate and the strain accommodated by faults over time. To account for the cratering rate, we calculated the areas associated with craters of each of the systems (see supporting information). As crater degradation stages are generally correlated with Mercury's stratigraphic systems [*Spudis and Guest*, 1988], only classes 1 and 2 craters would have been present prior to the Calorian, and by the end of the Calorian, all class 3 craters were emplaced. Preserved craters emplaced in the Pre-Tolstojan and Tolstojan occupied an area 4.62 times larger than that covered by Calorian craters. By the end of the Mansurian, all class 4 craters were emplaced and Calorian craters covered 3.25 times as much area as Mansurian craters, with the area ratio of Pre-Tolstojan/Tolstojan to Calorian craters being 4.60:1. This ratio is lower because craters emplaced in the Mansurian covered more area on Pre-Tolstojan and Tolstojan surfaces than on Calorian surfaces. At present, where class 5 craters are added to the total crater population, the Mansurian to Kuiperian crater area ratio is 19.15:1, the Calorian to Kuiperian crater area ratio is 62.31:1, and the Pre-Tolstojan/Tolstojan to Kuiperian crater area ratio is 286.53:1. The ratios of areas with respect to the Kuiperian result from the small size and frequency of craters in this time-stratigraphic system.

The crater area ratios provide a measure of the likelihood for a thrust fault population active during a given time-stratigraphic system to also have accommodated strain in craters that were already emplaced during any of the preceding systems. As impacts erase any pre-existing landforms, the strain expressed by a thrust fault-related landform inside a crater must have entirely been recorded after the crater was emplaced. Because we assume that crater area ratios are mostly consistent with global terrain ratios, they allow the calculation of the geometric probabilities for thrust faulting to accommodate strain within terrain associated with each of the time-stratigraphic systems. Combined with the previously established stratigraphic relationships, they then permit us to calculate the rate at which thrust faulting accommodated global contraction through time.

Out of the total population of studied craters, about 38% of Pre-Tolstojan/Tolstojan, 8.5% of Calorian, 1.5% of Mansurian, and 0% of Kuiperian craters are cut by thrust faults. These subpopulations of faults have the same slopes in their cumulative length distribution to one another and to the total fault population (see supporting information). This finding indicates that, despite differences in the absolute fault count in each of the fault subpopulations, each of the crater subpopulations is associated with the same ratio of small to long faults, so that the above percentages may be directly related to the strain accommodated within the cratered areas. Statistically, this means that 79.10% of the total population of thrust fault-related landforms mapped by *Byrne et al.* [2014] are expected to be associated with Pre-Tolstojan and Tolstojan terrains, 17.65% with Calorian, 3.25% with Mansurian, and 0% with Kuiperian terrains. For a total amount of 5.1 ± 2 km of radius change accommodated by thrust faults on Mercury [*Byrne et al.*, 2014], 4.0 ± 1.6 km are expected to be accommodated within Pre-Tolstojan/Tolstojan terrain and $0.90\,\text{km} \pm 0.35\,\text{km}$, 0.17 ± 0.07 km, and 0 km are expected to be accommodated within Calorian, Mansurian, and Kuiperian terrains, respectively. Importantly, these numbers of radius change are associated with faults present in the different terrains, but the faults themselves could have accommodated the strain at any time during and after the formation of these terrains. To deduce the actual amount of radius change per

time-stratigraphic system, we begin with estimating present-day contraction and cumulatively calculate our way backward through time.

From the observed timing relationships, there are no faults cutting Kuiperian craters, and so 0 km of Mercury's radius change is expressed in Kuiperian-aged terrains on the scale of observation of this study. In Mansurian terrain, ~0.17 ± 0.07 km of radius change is expected to be expressed by thrust faults, all of which must have been accommodated during that system. Accounting for the area ratios of all present craters during the Mansurian, geometric probabilities allow for up to ~0.54 ± 0.21 km of radius change accommodated by faults in Calorian terrain and ~2.47 ± 0.97 km radius change accommodated by faults in Pre-Tolstojan/Tolstojan terrain to also have occurred during the Mansurian (see supporting information), summing to a total of 3.18 ± 1.20 km of contraction (−0.13% ± 0.05% strain) likely being accommodated during that system.

Since 0.54 ± 0.21 km of the 0.9 ± 0.35 km of radius change expressed by faults in Calorian terrain are likely to already have occurred during the Mansurian and faults cutting Calorian craters do not express strain that occurred during the Pre-Tolstojan and Tolstojan systems, the remaining 0.36 ± 0.14 km of contraction associated with those faults must have been accommodated during the Calorian. Again, accounting for the area ratios of all studied craters that were present in the Calorian, geometric probabilities allow for up to 1.67 ± 0.65 km radius change accommodated by faults in Pre-Tolstojan/Tolstojan terrain to have occurred during the Calorian, summing to a total of 2.03 ± 0.79 km of contraction (−0.08% ± 0.03% strain) likely being accommodated during that system.

The cumulative amount of radius change accommodated during the Calorian and Mansurian systems equates to 5.21 ± 2.0 km, which is approximately equal to the amount of 5.1 ± 2 km that formed the basis of the calculations. This indicates that faults in Pre-Tolstojan/Tolstojan terrain accumulated displacements well after those periods and that no strain was accommodated by the mapped thrust faults during those early time systems. The discrepancy of our cumulative amount of radius change and the 5.1 km observed by *Byrne et al.* [2014] is likely a function of the onset of thrust faulting not coinciding with the Tolstojan/Calorian boundary, and this may indicate that thrust faulting was initiated somewhat after the beginning of the Calorian. This finding is consistent with our observations for the onset of global-contraction-induced thrust faulting taking place during the Calorian, with minimal, local thrust faulting activity occurring prior to this system. The calculated radius change of 2 km for the Calorian over a relatively short period of time and of 3 km for the Mansurian over a respectively long period of time supports the inference from the stratigraphic record (see section 2) that thrust faulting was very active during the Calorian compared to the thrust fault activity during Mansurian.

To quantify the change in strain for each time-stratigraphic system, i.e., the strain rate, we totaled the radius change accumulated during each system and related that amount to Mercury's initial radius and the length of time of each system (Figure 2). Recent estimates in lengths of Mercury's time systems using updated cratering chronologies for the inner solar system indicate a greater uncertainty of absolute ages, including much shorter Mansurian and Kuiperian systems [*Braden and Robinson*, 2013; *Banks et al.*, 2016]. We represent these ranges of lengths in time by using uncertainty regions surrounding our average strain rates (Figure 2, top row). During the Pre-Tolstojan and Tolstojan systems, strain accommodated prior to thrust faulting (0.3 to 2.1 km) could have accumulated over the entirety of these systems or in as little as 100 Ma [*Klimczak*, 2015]. The strain rates for this early time range from $5.4 \cdot 10^{-20}\,s^{-1}$ to $2.2 \cdot 10^{-19}\,s^{-1}$ (red dots, Figure 2). Our calculations show that Mercury's lithosphere experienced average strain rates of $4.1 \cdot 10^{-20} \pm 1.6 \cdot 10^{-20}\,s^{-1}$ during the Calorian (green dots, Figure 2) resulting in thrust fault formation, after which the strain rate slowed to $1.8 \cdot 10^{-20} \pm 0.7 \cdot 10^{-20}\,s^{-1}$ during the Mansurian (orange dots, Figure 2). This decrease in strain rate indicates that global contraction slowed considerably during the Mansurian. Higher initial strain rates would have translated to a fast radius decrease during and before the Calorian and a much slower radius decrease in the Mansurian (Figure 2, colored, gray, and gray dashed curves). Since no strain was resolved on the scale of our analysis for the Kuiperian, the radius decrease for this system is shown to drop to 0 km to indicate that global contraction, if still ongoing, has not substantially contributed to the strain and tectonic uplift accommodated by the large-scale thrust fault-related landforms on Mercury in its recent geologic history. *Byrne et al.* [2014], *Di Achille et al.* [2012], and *Watters et al.* [2013] estimate different amounts of radius change for Mercury. These three estimates produce different strain rates per time-stratigraphic system, but they all show the general pattern of a strain rate decrease over time (Figure 2).

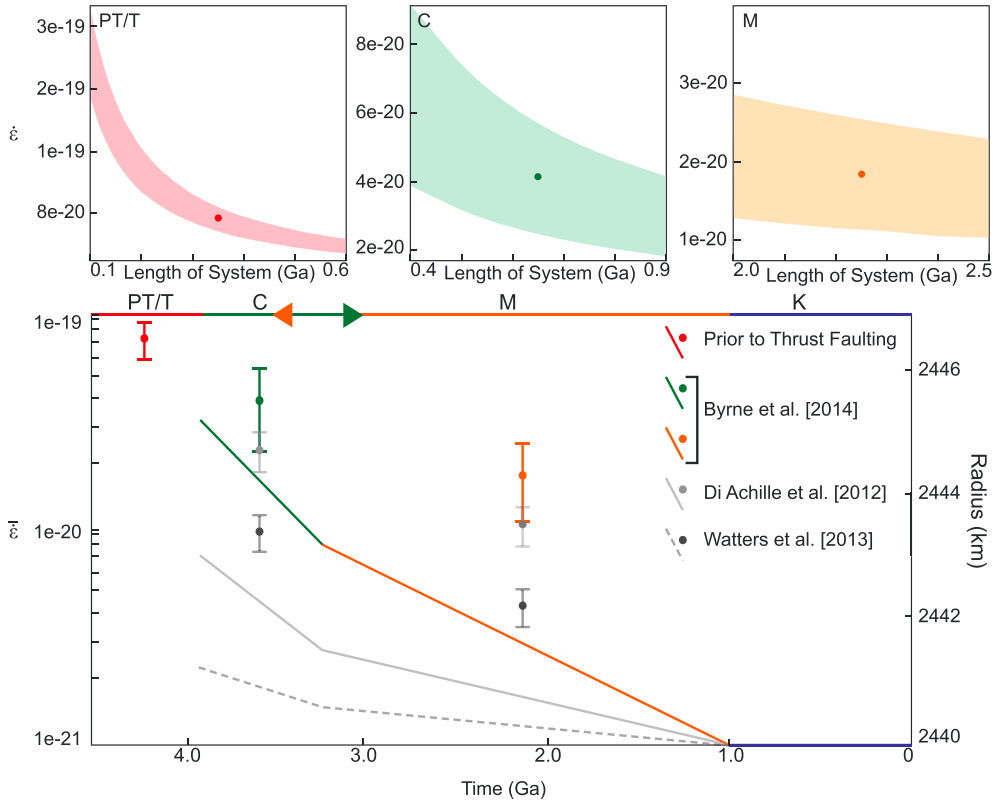

Figure 2. Timing and rate of Mercury's global contraction as a function of time before present, with time systems indicated as Pre-Tolstojan/Tolstojan = PT/T, Calorian = C, Mansurian = M, and Kuiperian = K. (top row) The red, green, and orange uncertainty regions bound strain rate estimates based on total radius change (7.1 km ≈ upper edge, 3.1 km ≈ lower edge [*Byrne et al.*, 2014]) and the length of time system (shortest ≈ left edge, longest ≈ right edge) [*Spudis and Guest*, 1988]. (bottom row) Average values for strain rates with respect to length of system and radius change are shown as darker points and correspond to colored points. Strain rate averages for *Byrne et al.* [2014] and those calculated for estimates from *Di Achille et al.* [2012] and *Watters et al.* [2013] are shown as dots in color, light gray, and dark gray, respectively. The curves show Mercury's radius expected from the start of the Calorian to present calculated from each of the three sets of estimates.

4. Implications

4.1. Implications for Slip Rates and Duration of Development of Thrust Fault-Related Landforms

We can utilize our calculated strain rates to gain insight into the time it took to build the observed fault-related topography. For example, Adventure Rupes, a thrust fault-related landform ~270 km-in-length and showing a topographic expression of ~1.3 km, has been dated to have formed during the Calorian by using crater counting techniques [*Banks et al.*, 2015b]. For that, the fault would have taken as little as 5 ± 1 Ma to build to its present structural relief. Similarly, Enterprise Rupes, a large fault-related landform with a length of ~800 km and a vertical relief of ~3 km, was previously dated by using buffered crater counting to date back to ~3.5–3.7 Ga [*Giacomini et al.*, 2015], or to the early Calorian, possibly predating the emplacement of the Rembrandt Basin [*Ferrari et al.*, 2015]. For this time frame, it would have taken about 45 ± 10 Ma to establish the present-day topography, if the fault system producing the landform was continuously active within the Calorian. *Ferrari et al.* [2015] estimated that if the fault system had been active prior to Rembrandt's emplacement, it might have been tectonically active for up to 200 Myr, which is broadly consistent with our estimate. Given that some faults have been found to cut young craters smaller than 20 km [*Banks et al.*, 2015a; *Watters et al.*, 2016], it is possible that fault growth has not been continuous, but instead included long periods of quiescence of tectonic activity and subsequent reactivation on Mercury's thrust faults.

Thrust fault growth on Mars has been compared to intraplate thrust faults on Earth with slip rates ~0.01–1 mm/yr and strain rates between 10^{-17} and 10^{-19} s^{-1} [*Schultz*, 2003]. Faults on Mercury likely grew at comparable rates during the Calorian, where we estimate slip rates for Adventure and Enterprise Rupes

to fall between 0.1 mm/yr and 0.4 mm/yr with strain rates at around $10^{-20}\,s^{-1}$. During this system, Mercury quakes may have been on the order of 100 quakes with surface wave magnitudes between 3 and 7 per 10 year period, similar to the frequency of Mars quakes estimated from strain rates of ~$10^{-19}\,s^{-1}$ due to global and lithospheric cooling [*Phillips*, 1991]. For slower strain rates in the Mansurian and Kuiperian, and consequently lower slip rates of thrust faults, Mercury quakes triggered by global contraction are likely rare events.

4.2. Implications for Mercury's Thermal Evolution

The magnitude and onset time of global contraction as well as its rate as a function of time can provide important geologic bounds for thermal models and thus for the evolution of Mercury's interior. Most models for Mercury's thermal history recognize two stages of radius evolution: radial growth due to planetary heating and contraction due to cooling [e.g., *Hauck et al.*, 2004; *Grott et al.*, 2011; *Tosi et al.*, 2013]; however, some only allow for contraction with more subdued contraction during initial phases [e.g., *Grott et al.*, 2011]. These models often convey results through radius change curves. These curves have positive slopes caused by interior heating and global expansion before peaking and then display negative slopes due to interior cooling and global contraction. Our radius change curves, shown in Figure 2, account for rates of contraction-induced thrust faulting during the cooling period of Mercury's thermal history and thus have overall negative slopes. Many thermal evolution models display relatively constant radius change following prolonged expansion or periods of little radius change.

While the early phase of expansion is not characterized in this study, the most recent time at which this phase ended must fall prior to the onset time of global contraction-induced thrust faulting. This time and the time derivative of global contraction, represented by the shape of the negative slope—a function of the strain rate—are both constrained with geologic observations of this study (Figure 2). Multiple lines of evidence point to an onset time of global contraction-induced thrust faulting during the Calorian, which, for established crater chronologies, may be as early as 3.9 Ga ago [*Spudis and Guest*, 1988]. This shows that global contraction may have operated much earlier than many of the thermal models predict. After the onset of global contraction, thrust faulting operated at its fastest rate. The process slowed during the Mansurian and slowed even further during the Kuiperian (Figure 2, colored and solid and dashed gray lines). Our results allow future thermal evolution models to be constrained by and assessed with these geologic findings.

5. Conclusions

Stratigraphic relationships of faults and craters of different degradation stages were used to interpret Mercury's history of global contraction. Heavily degraded, older craters covering a higher portion of surface area on Mercury tend to be crosscut by thrust faults, whereas fresh, younger craters cover a smaller area but tend to superpose thrust fault-related landforms. Quantification of these relationships allowed us to derive the geometric probabilities for thrust faults to cut craters through time and to relate this finding to the onset time and strain rates of thrust faulting that resulted from global contraction. Our results indicate that global contraction likely began prior to the Calorian, but that thrust faults did not begin to accommodate shortening until the early Calorian. Calculated strain rates show that global contraction slowed toward present day. These results provide geologically constrained estimates of Mercury's timing and rate of contraction, which may serve to check the plausibility of thermal evolution models of the planet. They also advise our interpretations of landform development and slip rates, with the largest faults having the potential to have grown in as little as 50 Ma.

Acknowledgments
We thank Mallory Kinczyk, Caleb Fassett, and Louise Prockter for providing helpful input with the crater classification. This manuscript benefitted from detailed and thoughtful comments from two anonymous reviewers. The methods and data used to produce the results of this paper are derived from freely available sources in the published literature and planetary data system. Data sets and computer code to generate our results are provided in the supporting information. Global thrust fault data set is available from *Byrne et al.* [2014].

References

Banks, M. E., Z. Y. Xiao, T. R. Watters, R. G. Strom, S. E. Braden, C. R. Chapman, S. C. Solomon, C. Klimczak, and P. K. Byrne (2015a), Duration of activity on lobate-scarp thrust faults on Mercury, *J. Geophys. Res. Planets*, *120*, 1751–1762, doi:10.1002/2015JE004828.

Banks, M. E., N. Barlow, C. Klimczak, Z. Xiao, T. R. Watters, and C. R. Chapman (2015b), Duration of activity on lobate-scarp thrust faults on Mercury, *Planet. Crater Consort.*, *6*, 1513.

Banks, M. E., Z. Xiao, S. E. Braden, S. Marchi, C. R. Chapman, N. G. Barlow, and C. I. Fassett (2016), Revised age constraints for Mercury's Kuiperian and Mansurian systems, *Lunar Planet. Sci. Conf.*, *47*, 2943.

Barnouin, O. S., M. T. Zuber, D. E. Smith, G. A. Neumann, R. R. Herrick, J. E. Chappelow, S. L. Murchie, and L. M. Prockter (2012), The morphology of craters on Mercury: Results from MESSENGER flybys, *Icarus*, *219*, 414–427, doi:10.1016/j/icarus.2012.02.029.

Braden, S. E., and M. S. Robinson (2013), Relative rates of optical maturation of regolith on Mercury and the Moon, *J. Geophys. Res. Planets*, *118*, 1903–1914, doi:10.1002/jgre.20143.

Byrne, P. K., Klimczak, C., Sengor, A. M. C., Solomon, S. C., Watters, T. R., and S. A. Hauck (2014), Mercury's global contraction much greater than earlier estimates, *Nat. Geosci.*, *7*, 301–307, doi:10.1038/ngeo2097.

Cowie, P. A., and C. H. Scholz (1992), Growth of faults by accumulation of seismic slip, *J. Geophys. Res.*, *97*, 11,085–11,095, doi:10.1029/92JB00586.

Di Achille, G., C. Popa, M. Massironi, E. M. Epifani, M. Zusi, G. Cremonese, and P. Palumbo (2012), Mercury's radius change estimates revisited using MESSENGER data, *Icarus*, *221*, 456–460, doi:10.1016/j.icarus.2012.07.005.

Ferrari, S., M. Massironi, S. Marchi, P. K. Byrne, C. Klimczak, E. Martellato, and G. Cremonese (2015), Age relationships of the Rembrandt Basin and Enterprise Rupes, Mercury, *Geol. Soc. London Spec. Publ.*, *401*, 159–172, doi:10.1144/SP401.20.

Giacomini, L., M. Massironi, S. Marchi, C. I. Fassett, G. Di Achille, and G. Cremonese (2015), Age dating of an extensive thrust system on Mercury: Implications for the planet's thermal evolution, *Geol. Soc. London Spec. Publ.*, *401*, 291–311, doi:10.1144/SP401.21.

Grott, M., D. Breuer, and M. Laneuville (2011), Thermo-chemical evolution and global contraction of Mercury, *Earth Planet. Sci. Lett.*, *307*, 135–146, doi:10.1016/j.epsl.2011.04.040.

Hauck, S. A., A. J. Dombard, R. J. Phillips, and S. C. Solomon (2004), Internal and tectonic evolution of Mercury, *Earth Planet. Sci. Lett.*, *222*, 713–728, doi:10.1016/j.epsl.2004.03.037.

Kinczyk, M. J., L. M. Prockter, C. R. Chapman, and H. C. M. Susorney (2016), A morphological evaluation of crater degradation on Mercury: Revisiting crater classification using MESSENGER data, *Lunar Planet. Sci. Conf.*, *47*, 1573.

Klimczak, C. (2015), Limits on the brittle strength of planetary lithospheres undergoing global contraction, *J. Geophys. Res. Planets*, *120*, 2135–2151, doi:10.1002/2015JE004851.

Marchi, S., C. R. Chapman, C. I. Fassett, J. W. Head, W. F. Bottke, and R. G. Strom (2013), Global resurfacing of Mercury 4.0–4.1 billion years ago by heavy bombardment and volcanism, *Nature*, *499*, 59–61, doi:10.1038/nature12280.

Mccauley, J. F., J. E. Guest, G. G. Schaber, N. J. Trask, and R. Greeley (1981), Stratigraphy of the Caloris Basin, Mercury, *Icarus*, *47*, 184–202, doi:10.1016/0019-1035(81)90166-4.

Morbidelli, A., S. Marchi, W. F. Bottke, and D. A. Kring (2012), A sawtooth-like timeline for the first billion years of lunar bombardment, *Earth Planet. Sci. Lett.*, *355*, 144–151, doi:10.1016/j.epsl.2012.07.037.

Phillips, R. J. (1991), Expected rates of Mars quakes: Scientific rational and requirements for a global seismic network on Mars, in *Scientific Rationale and Requirements for a Global Seismic Network on Mars*, *Tech. Rep.*, pp. 35–38, LPI, Houston, Tex.

Schultz, R. A. (2003), Seismotectonics of the Amenthes Rupes thrust fault population, Mars, *Geophys. Res. Lett.*, *30*(6), 1303, doi:10.1029/2002GL016475.

Solomon, S. C. (1977), The relationship between crustal tectonics and internal evolution in the Moon and Mercury, *Phys. Earth Planet. Inter.*, *15*, 135–145, doi:10.1016/0031-9201(77)90026-7.

Spudis, P. D., and J. E. Guest (1988), Stratigraphy and geologic history of Mercury, in *Mercury*, edited by F. Vilas, C. R. Chapman, and M. S. Matthews, pp. 118–164, Univ. of Ariz. Press, Tuscon.

Strom, R. G., and G. Neukum (1988), The cratering record on Mercury and the origin of impacting objects, in *Mercury*, edited by F. Vilas, C. R. Chapman, and M. S. Matthews, pp. 336–373, Univ. of Ariz. Press, Tuscon.

Tosi, N., M. Grott, A. C. Plesa, and D. Breuer (2013), Thermochemical evolution of Mercury's interior, *J. Geophys. Res. Planets*, *118*, 2474–2487, doi:10.1002/jgre.20168.

Trask, N. J. (1967), Distribution of Lunar craters according to morphology from Ranger VIII and IX photographs, *Icarus*, *6*, 270–276, doi:10.1016/0019-1035(67)90023-1.

Trask, N. J. (1971), Geologic comparison of Mare materials in the Lunar equatorial belt, including Apollo 11 and Apollo 12 landing sites, U.S. Geol. Survey Prof. Pap. 750-D, D138—D144, Washington, D. C.

Trask, N. J., and J. E. Guest (1975), Preliminary geologic terrain map of Mercury, *J. Geophys. Res.*, *80*, 2461–2477, doi:10.1029/JB080i017p02461.

Watters, T. R., et al. (2013), Distribution of prominent lobate scarps on Mercury: Contribution to global radial contraction, *Lunar Planet. Sci. Conf.*, *44*, 1719.

Watters, T. R., M. M. Selvans, M. E. Banks, S. A. Hauck, K. J. Becker, and M. S. Robinson (2015), Distribution of large-scale contractional tectonic landforms on Mercury: Implications for the origin of global stresses, *Geophys. Res. Lett.*, *42*, 3755–3763, doi:10.1002/2015GL063570.

Watters, T. R., K. Daud, M. E. Banks, M. M. Selvans, C. R. Chapman, and C. M. Ernst (2016), Recent tectonic activity on Mercury revealed by small thrust fault scarps, *Nat. Geosci.*, *9*, 743–747, doi:10.1038/ngeo2814.

Wood, C. A., Head, J. W., and M. J. Cintala (1977), Crater degradation on Mercury and the Moon: Clues to surface evolution, paper presented at Lunar Science Conference, Houston, Tex.